WELDING RESEARCH

SUPPLEMENT TO THE *WELDING JOURNAL*, APRIL 1988

Sponsored by the American Welding Society and the Welding Research Council

All papers published in the *Welding Journal's* Welding Research Supplement undergo Peer Review before publication for: 1) originality of the contribution; 2) technical value to the welding community; 3) prior publication of the material being reviewed; 4) proper credit to others working in the same area; and 5) justification of the conclusions, based on the work performed.

The names of the more than 170 individuals serving on the AWS Peer Review Panel are published periodically. All are experts in specific technical areas, and all are volunteers in the program.

A Study of Heat-Affected Zone and Weld Metal Liquation Cracking in Alloy 903

A greater incidence of cracking was observed in the weld metal in comparison to the HAZ

BY W. A. BAESLACK III, W. P. LATA AND S. L. WEST

ABSTRACT. The heat-affected zone and weld metal liquation cracking characteristics of the high-strength, low-expansion superalloy 903 have been examined using the Spot-Varestraint weldability test. Quantitative analysis of cracking found liquation cracking susceptibility of the Alloy 903 weld metal to be significantly greater than that of the solution-annealed base metal. Extensive regions of partial melting were observed in both the base metal and weld metal HAZ regions, with liquation attributed primarily to the constitutional liquation of Nb-rich carbides in the base metal and Laves phase in the weld metal. Both eutectic liquation reactions resulted in the formation of a low-melting austenite/Laves eutectic at grain boundaries, which served as the precursor to liquation cracking. The greater liquation cracking sensitivity of the weld metal was attributed to: 1) a lower eutectic reaction temperature of the Laves phase versus the Nb-rich carbides, 2) a coarser austenitic grain size, and 3) a less tortuous intergranular crack path.

W. A. BAESLACK III and S. L. WEST are with the Department of Welding Engineering, The Ohio State University, Columbus, Ohio. W. P. LATA is with Amatek-Straza, El Cajon, Calif.

Introduction

Alloy 903 is a precipitation-strengthened, low-coefficient-of-thermal-expansion (low-COE) Fe-Ni-Co alloy designed for elevated temperature applications requiring high strength and superior resistance to thermal fatigue (Refs. 1, 2). The excellent room and elevated temperature strengths exhibited by the alloy result from the presence of Al, Ti and Nb (about 7 total wt-%), which promote formation of the gamma-prime $Ni_3(Al, Ti)$ strengthening phase. The highly desirable combination of properties offered by Alloy 903 has promoted its increased use in aerospace applications that require close tolerance control over a wide range of temperatures. In addition, a high resistance to hydrogen environmental embrittlement has led to utilization of the alloy as a cladding material for conventional Ni-base superalloys, such as Alloy 718 (Ref. 2).

KEY WORDS

Liquation Cracking
Weld Metal Liquation
Superalloy 903
HAZ Liquation
Nb-rich Carbides
Laves Phase
Constitutional Liquation
Laves Eutectic
Crack Susceptibility
Spot-Varestraint Test

During the past decade, numerous investigators have shown that fully austenitic Fe- and Ni-base alloys that contain Nb or Ti can be highly susceptible to liquation cracking (Refs. 3–7). This form of weld cracking involves the formation of a thin liquid film at the heat-affected zone (HAZ) grain boundaries during the weld heating cycle and the inability of this film to accommodate thermally and/or mechanically induced stresses experienced during cooling. It can occur both in the base metal adjacent to the fusion line (designated as "HAZ" liquation cracking) and in underlying passes of multipass welds or cladding (designated as "weld metal" liquation cracking[1]) (Ref. 8). In Nb- and Ti-containing alloys, the liquation

[1]*Note that if liquation cracking in an underlying pass and fusion solidification cracking both occur due to the presence of the same low-melting film at grain boundaries, the combined cracking phenomena may be singularly described as solidification cracking (Ref. 8).*

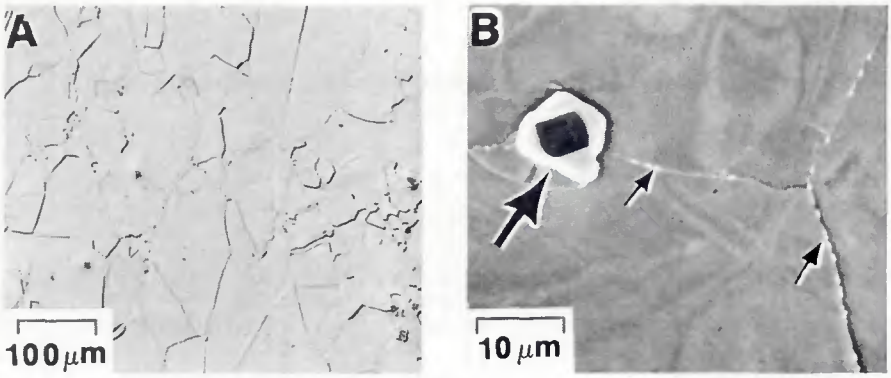

Fig. 1—Micrographs of solution-annealed Alloy 903 microstructure. A—Light microscope; B—SEM. Large arrow indicates coarse, Nb-rich MC carbide. Small arrows indicate fine, Nb-rich carbides at austenitic grain boundaries. Note the presence of Ti-rich carbonitride (dark) at center of coarse carbide

phenomenon, which serves as a prerequisite for cracking, has been attributed to several different mechanisms, including the constitutional liquation (eutectic liquation) of Nb- and Ti-rich carbides (Refs. 3–6) and the "sweeping up" of free titanium residual in the matrix from the dissolution of Ti-rich carbides (Ref. 7).

Based on the comparatively high level of Nb + Ti in Alloy 903, liquation cracking might be anticipated. Recent weld cladding studies of Alloy 903 on Alloy 718 have indeed indicated significant difficulties with underbead cracking in multipass deposits (Ref. 9). The intergranular cracking morphology and evidence of incipient melting at grain boundaries in the cladding microstructures strongly suggested a weld metal liquation cracking phenomenon.

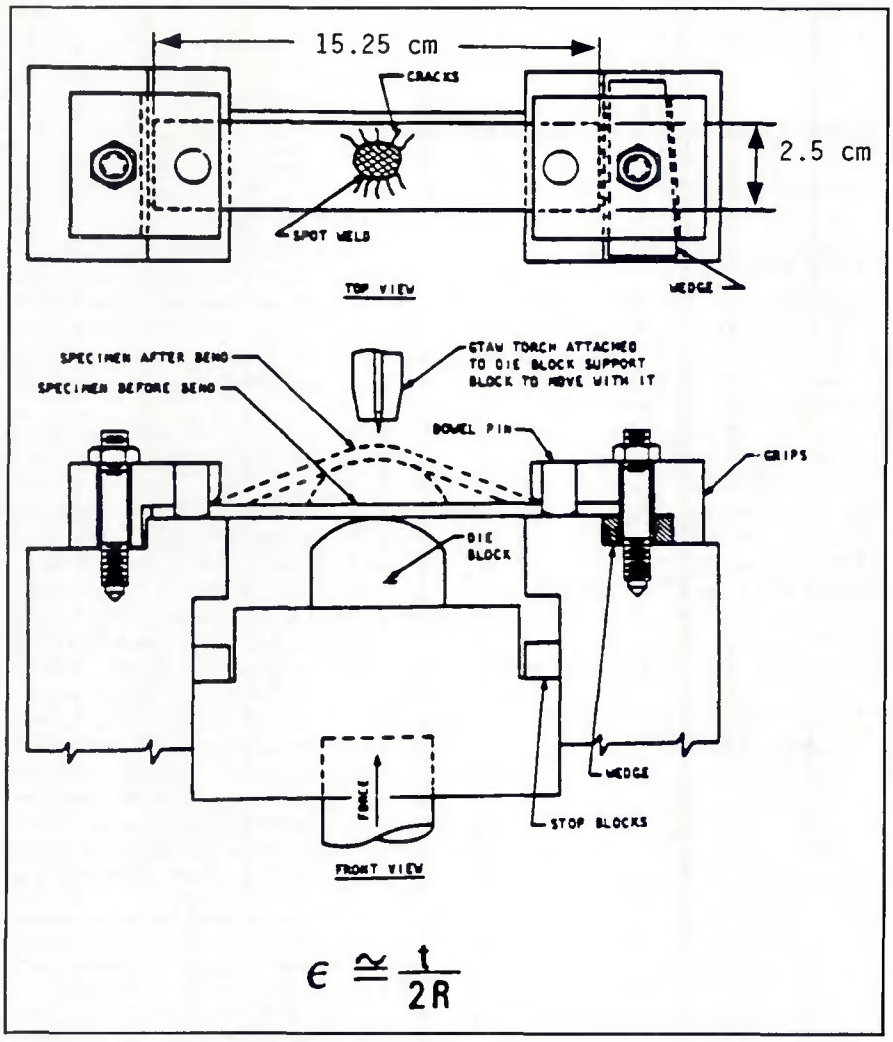

Fig. 2—Schematic illustration of Spot-Varestraint test apparatus

The aerospace industry is presently expanding their application of both Alloy 903 and next-generation low-COE alloys (*e.g.*, 907 and 909) of similar composition and structure. Therefore, it would be desirable to have an improved understanding of both the weld and HAZ liquation cracking phenomena of this alloy and how they compare to similar structural alloys.

The objectives of the present investigation are threefold: 1) to quantitatively evaluate the HAZ and weld metal liquation cracking sensitivities of Alloy 903, 2) to characterize the weld microstructures and cracking morphologies, and 3) to identify the metallurgical mechanisms responsible for the liquation and cracking phenomena.

Experimental Procedure

Material

A commercial heat of Alloy 903 in the form of 6.4-mm (0.25-in.) thick plate was investigated. The chemical composition is provided in Table 1. Figure 1 illustrates the nearly equiaxed austenitic grain structure (ASTM grain size 6) characteristic of the solution-annealed (940°C/1724°F, 1 h, WQ) condition. Microstructural examination at increased magnification using a scanning electron microscope (SEM) showed a bimodal distribution of carbides throughout the microstructure. Coarse, Nb-rich carbides, which originated from ingot solidification, were located randomly in the microstructure. Occasionally, Ti-rich carbonitrides were also observed in the matrix, and they often appeared to serve as nuclei for the coarse, Nb-rich carbides—Fig. 1B. Much finer Nb-rich carbides, which formed during annealing, were observed to decorate austenitic grain boundaries.

Weldability Testing

Quantitative analysis of the weld metal and HAZ liquation cracking susceptibilities was accomplished by Spot-Varestraint testing (Ref. 10). This simulative weldability test utilized the apparatus schematically illustrated in Fig. 2 and test specimens with dimensions of 15.2 × 2.5 × 0.65 cm (6.0 × 1.0 × 0.25 in.). In addition to all-base-metal specimens, "double-weld" specimens were also prepared for evaluation of weld metal liquation cracking. A schematic illustration of these double-weld specimens is shown in Fig. 3. As will be discussed in a subsequent section, the location of the continuous GTA weld, with respect to the GTA spot weld, was an important consideration in obtaining comparable quantitative results of cracking susceptibility. Welding parameters for the continuous GTA weld are listed in

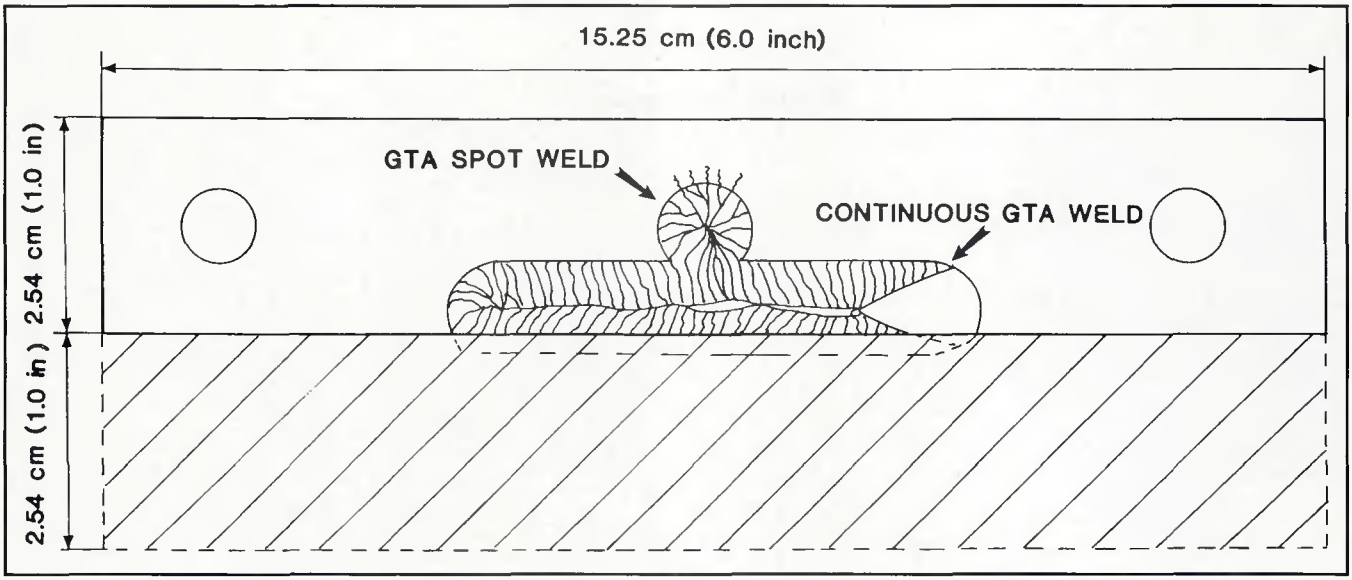

Fig. 3 — Schematic illustration describing preparation of double-weld Spot-Varestraint test specimen. The area indicated by cross-hatching was removed prior to testing, but was present during continuous GTA welding

Table 2.

During Spot-Varestraint testing, a gas tungsten arc spot weld was produced for a duration of 15 s, thereby allowing the thermal conditions in the weld region and the weld pool diameter to stabilize and approach steady state. After this period, the arc was extinguished, and a ram was actuated, impinging the specimen and forcing it to conform around a die block of predetermined radius. A delay time of 100 ms between the arc shutoff and ram impingement was employed in order to confine cracking to the HAZ. Spot-Varestraint test parameters are shown in Table 2. Augmented strain levels of 1, 2 and 3% were employed.

Subsequent to testing, the specimens were examined using a binocular microscope at 50X magnification in order to measure the total number of cracks and the length of each crack. A minimum of three specimens were tested for each condition and strain level. Note that for the double-weld specimens, the total number of cracks and the total crack length on the weld and HAZ sides of the specimens were tabulated independently and doubled for comparative purposes.

Structure Characterization

Representative test specimens were sectioned and mounted in bakelite for metallographic characterization. After polishing through 0.05 micron alumina, the microstructure was revealed using an etchant consisting of equal parts concentrated nitric, hydrochloric and lactic acids. Examination of the polished and etched specimens included both light and SEM microscopy. Phase compositions were determined using energy-dispersive x-ray analysis (EDS). Fracture surfaces of both HAZ and weld metal liquation cracks were exposed by careful sectioning and were examined using SEM/EDS analysis.

Results

Macroscopic Cracking Characteristics

Figures 4A–D illustrate HAZ and weld metal liquation cracks in a double-weld Spot-Varestraint specimen tested at 3% augmented strain. As shown, the cracks propagated approximately perpendicular to the fusion line and generally did not extend into the fusion zone of the spot weld. It is important to note that the weld metal liquation cracks were confined primarily to boundaries of the transverse-oriented, columnar grains in the continuous GTA weld. However, in several initial test specimens, cracks were observed to be either blunted by continuous, longitudinal grain boundaries at the weld centerline (Fig. 5A), or bifurcated by equiaxed dendrites in this region — Fig. 5B. These effects were found to influence the quantitative cracking analysis, particularly in reducing the maximum crack length. Consequently, only specimens exhibiting cracks exclusively within the columnar region were considered in the following quantitative analysis of cracking susceptibility.

Quantitative Analysis of Cracking Susceptibility

Figures 6 and 7 illustrate plots of total crack length (TCL) and total number of cracks versus percent augmented strain

Table 1—Chemical Composition of Alloy 903 (wt-%)

Fe	Ni	Co	Nb	Ti	Al	Cu	Cr	Si	C	S
bal.	37.79	14.83	2.87	1.37	0.96	0.39	0.22	0.13	0.02	0.001

Table 2—Parameters for Continuous GTA Welding and Spot-Varestraint Testing

	Continuous GTA Welding	Spot-Varestraint Testing
Current	325 A	125 A
Voltage	10 V, DCEN	10–11 V, DCEN
Travel rate	2.5 mm/s (6 ipm)	NA
Electrode	2.38 mm (0.094 in.) W-ThO 30-deg included angle	2.38 mm (0.094 in.) W-ThO 30-deg included angle
Electrode-to-work-distance	1.5 mm (0.060 in.)	1.5 mm (0.060 in.)
Arc time	NA	15 s
Delay time	NA	100 ms
Shielding	Argon, 15.3 L/s (20 cfh)	Argon, 15.3 L/s (20 cfh)

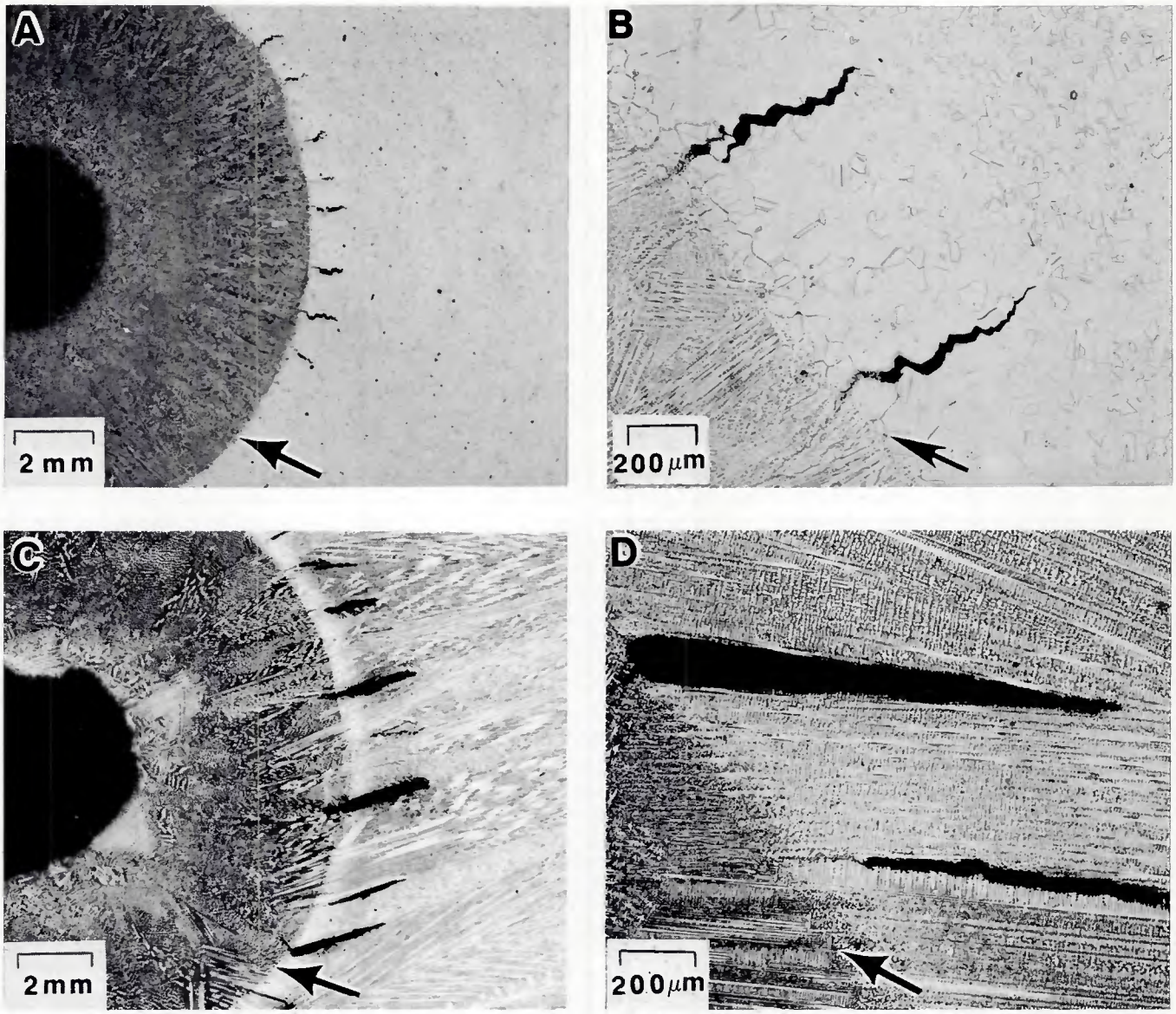

Fig. 4 — Macrographs of double-weld Spot-Varestraint specimen tested at 3% augmented strain. A and B — Base metal side; C and D — continuous GTA weld fusion zone side. Arrows indicate GTA spot weld fusion line

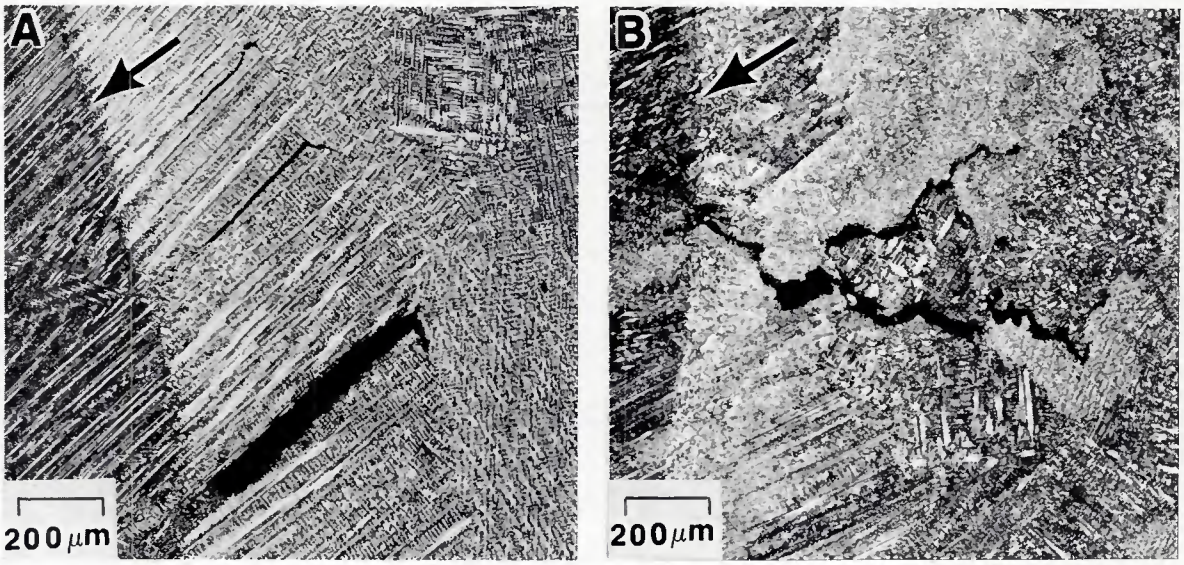

Fig. 5 — Weld metal liquation cracks in double-weld Spot-Varestraint specimen tested at 3% augmented strain. A — Crack deviation at longitudinal centerline grain boundary; B — crack bifurcation around equiaxed grain at weld centerline. Arrows indicate GTA spot weld fusion line

for the single and double-weld Alloy 903 Spot-Varestraint test specimens. Variations in the TCL data obtained for identical test conditions are indicated by scatter bands and were typical of those observed with Varestraint testing. It is of interest to note that both the TCL and the total number of cracks observed in the single-weld specimens were slightly higher than for the base metal side of the double-weld specimens. This was originally attributed to the effects of the thermal cycle experienced during production of the continuous GTA weld on the base metal microstructure, thereby increasing its sensitivity to cracking. Microstructural analysis, however, failed to reveal any changes in this region. In addition, monitoring of this location with thermocouples during continuous GTA welding showed a peak temperature of only 560°C (1040°F), which was too low to promote significant microstructural changes. An alternate explanation may be that the influence of compressive residual stresses produced in the specimen during continuous GTA welding induced the cracking during spot-Varestraint testing. Although the specimens exhibited negligible distortion after GTA welding (a benefit of the alloy's low-COE properties), it is possible that sufficient residual stresses existed to influence the cracking behavior.

A significantly greater susceptibility of Alloy 903 to weld metal, as opposed to HAZ liquation cracking, is indicated by Figs. 6 and 7. Although not graphically illustrated, values for maximum crack length (MCL) paralleled those for TCL. Average MCL values for double-weld HAZ, single-weld and double-weld fusion zone specimens tested at 3% augmented strain were 0.48, 0.57 and 1.12 mm (0.018, 0.022 and 0.044 in.), respectively.

Microstructure Characterization

Light microscopy clearly revealed the existence of appreciable heat-affected and partially melted regions in the GTA spot welds—Fig. 4C. However, SEM/EDS analysis was required to more clearly delineate the metallurgical phenomena associated with these regions. Figure 8A illustrates the fine, equiaxed austenitic grain structure present in the far heat-affected zone of a single-weld Spot-Varestraint test specimen. A grain size appreciably finer than that observed in the unaffected base metal and the location of fine carbides exclusively at prior austenitic grain boundaries indicated recrystallization in this region. The driving force for such recrystallization in a solution-annealed microstructure was not apparent. However, its occurrence in unrestrained continuous and spot GTA welds showed the phenomenon not to be an artifact of the Spot-Varestraint test. Higher peak temperatures experienced in the near HAZ promoted simultaneous solid-state dissolution of the fine, Nb-rich carbides and austenitic grain growth.

The transition from the true HAZ to a partially melted region was characterized by the onset of liquation at the interface between the coarse, Nb-rich carbides and the austenitic matrix—Fig. 8B. The extent of this liquation reaction increased nearer the fusion line (Fig. 8C), and within

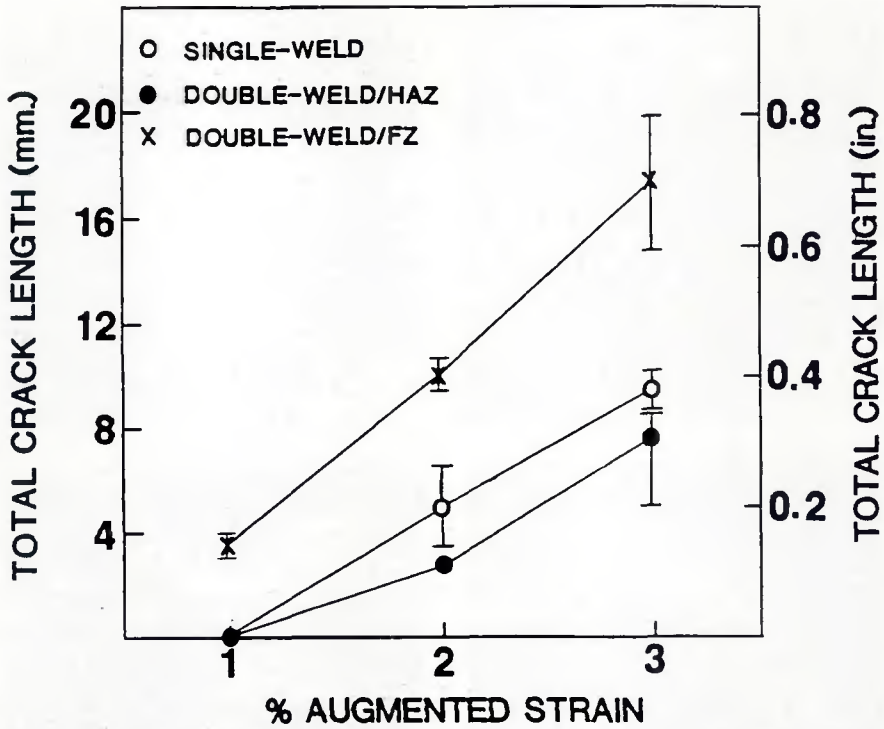

Fig. 6—Plot of total crack length versus percent of augmented strain for Spot-Varestraint-tested single and double-weld specimens. Note that values for each side of double-weld specimens are doubled for comparative purposes

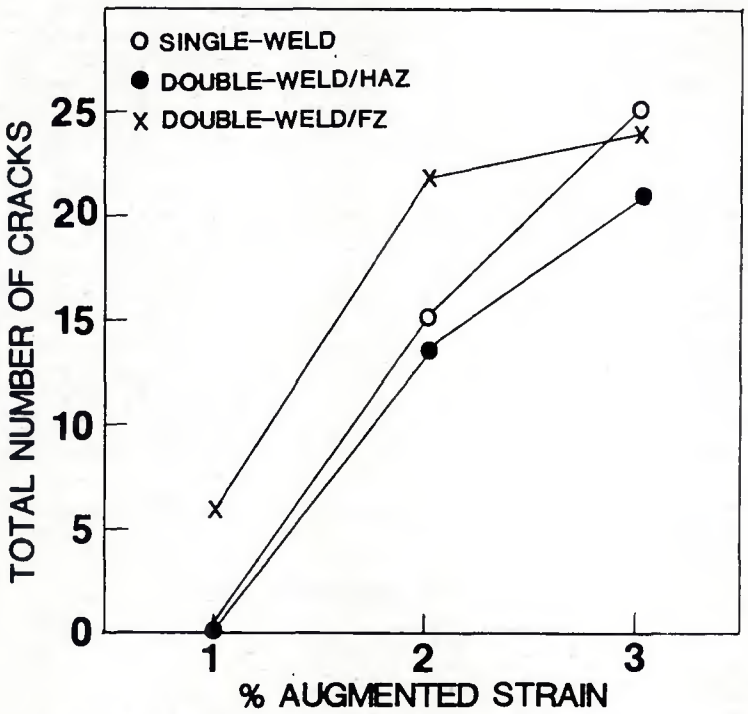

Fig. 7—Plot of total number of cracks versus percent of augmented strain for Spot-Varestraint-tested single and double-weld specimens. Note that values for each side of double-weld specimens are doubled for comparative purposes

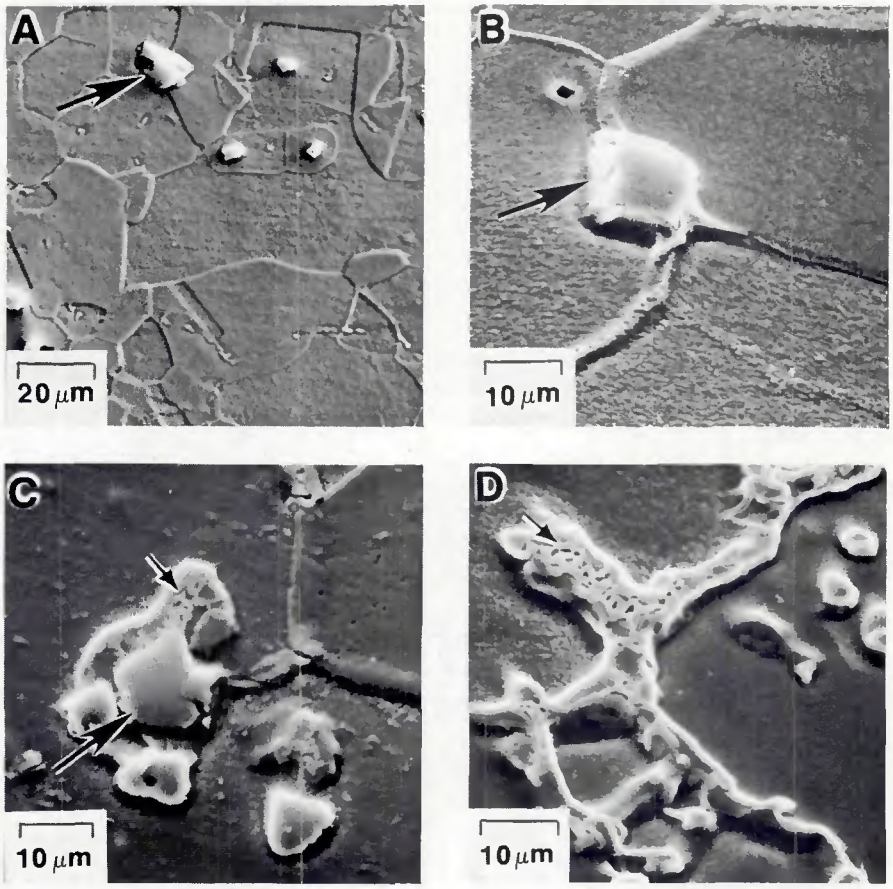

Fig. 8—SEM micrographs of heat-affected and partially melted zones in single-weld Spot-Varestraint test specimen. A—Recrystallized austenitic grains in HAZ; B—onset of carbide liquation in far PMR; C—more extensive carbide liquation in PMR; D—complete grain boundary liquation adjacent to fusion line. Large arrows indicate Nb-rich carbides. Small arrows indicate Laves phase in resolidified product

a few grain diameters of the fusion line, carbide dissolution appeared complete. As shown in Fig. 8D, grain boundaries adjacent to the fusion line were heavily liquated. Examination of the resolidified products surrounding decomposed carbides (Fig. 8C) and at liquated grain boundaries revealed a secondary constituent phase. Although definitive phase analysis (*e.g.*, x-ray diffractometry or TEM electron diffraction) was not performed, morphological considerations strongly suggested that the constituent was a Laves phase similar to that previously observed in Fe- and Ni-base superalloys (*e.g.*, Alloy 718 and A-286). Semi-quantitative EDS analyses at pertinent locations in the partially melted region are shown in Table 3. The Laves phase chemistry exhibited a Nb + Ti concentration somewhat below that expected for an $(Fe,Co,Ni)_2$ (Nb,Ti) Laves phase stochiometry. This may be explained by the fine scale of the Laves phase, which precluded precise chemical analysis (resolution in bulk electron microanalytical techniques is generally limited to 1 micron). In addition, the possibility that some Fe, Co and/or Ni substituted for either Nb or Ti in the Laves structure may also account for the lower Nb + Ti levels.

HAZ liquation cracking occurred intergranularly in the far partially melted region. The cracks generally exhibited irregular edges and variations in width, which are typical of liquation versus solid state ductility-dip cracking. As illustrated in Fig. 4B and 9A, the austenitic grain boundaries adjacent to the cracks showed little or no evidence of liquation, suggesting the presence of an extremely thin film of liquid at these boundaries during cracking. Also shown in Fig. 9 is extensive backfilling of the crack opening adjacent to the fusion zone (Fig. 9B) and at the crack tip (Fig. 9C) by liquid from the fusion zone or from heavily liquated grain boundaries in the near partially melted region. A significant enrichment of this backfilled liquid in Nb was evidenced by its solidification to the austenite/Laves phase eutectic.

The teardrop-shaped pool exhibited by the continuous GTA weld promoted the formation of a columnar fusion zone grain structure. On a microscopic scale, solidification occurred to primary austenite by a cellular dendritic mode. As shown in Fig. 10, microsegregation of principally Nb and Ti to intergranular and interdendritic regions during solidification promoted the formation of a cored austenitic structure and solidification of the final liquid to an austenite/Laves phase eutectic. Backscattered electron imaging of the secondary constituent particles at cellular dendritic interstices also indicated the presence of fine carbides, suggesting the occurrence of a second eutectic reaction during the final stages of solidification. Unfortunately, these particles were too small for identification using SEM/EDS analysis.

Examination of the continuous GTA weld fusion zone adjacent to the spot weld fusion line showed both heat-affected and partially melted regions. In the heat-affected zone, temperatures were sufficiently high to promote partial homogenization of the cored austenitic structure, while not visibly affecting the morphology of the secondary constituent phases—Fig. 1A. Nearer the fusion line, extensive partial melting was observed both intergranularly and at cellular dendritic interstices—Figs. 11A and 11B. Although not as distinct as HAZ liquation, the SEM indicated that Laves phase at these locations had constitutionally liquated and resolidified back to the austenite/Laves eutectic on cooling.

Figures 4C and 4D and Fig. 11 illustrate the weld metal liquation cracks in a double-weld Spot-Varestraint specimen. As with HAZ liquation cracks, intergranular weld metal liquation cracks were characterized by extensive backfilling with Nb-rich liquid that solidified to the austenite/Laves eutectic.

Table 3—EDS Analysis of Alloy 903 Weld Haz[a]

	Chemical Composition (wt-%)				
Structure	Ni	Co	Nb	Ti	Fe
Matrix gamma	38.2	16.1	1.5	1.0	bal.
Ti-rich carbonitride	1.5	0	2.6	92.8	bal.
Coarse MC carbide	7.1	3.4	67.5	11.1	bal.
Laves	37.5	14.6	22.7	4.0	bal.
Eutectic gamma	39.7	15.1	7.3	3.0	bal.

(a) 30 kV, 100 Å, beam size, standardless analysis, average of several locations in each structure.

Fractographic Analysis

Figure 12 illustrates the surfaces of HAZ and weld metal liquation cracks. At locations on the surfaces farthest from the fusion line, distinctly intergranular fracture

surfaces were observed (Figs. 12A and 12C). Examination of these surfaces at high magnification showed fine, rippled or wavy patterns indicative of liquation versus solid-state ductility-dip fracture (Ref. 11). Approaching the fusion line, the surfaces appeared increasingly dendritic (Figs. 12B and 12D), indicative of increased liquid at grain boundaries in this region. Microstructural examination of both HAZ and weld metal liquation crack surfaces showed varying degrees of Nb enrichment when compared to the nominal alloy chemistry. In addition, Laves phase was commonly observed on the crack surfaces.

Discussion

Cracking Susceptibility

A comparison of Spot-Varestraint test data (TCL versus augmented strain), obtained in the present investigation with that reported by other investigators for austenitic Fe- and Ni-base alloys containing Ti and/or Nb, is shown in Fig. 13. As indicated, the solution-annealed Alloy 903 exhibited a somewhat greater susceptibility than the Fe-base alloys A-286 (Ref. 4) and 800 (Ref. 7) in comparable solution-annealed conditions, particularly at the higher augmented strains. Although a direct comparison with solution-annealed Alloy 718 was not possible, Alloy 903 did show a HAZ cracking susceptibility similar to Alloy 718 (Ref. 12) in the solution heat-treated and aged condition.[2] It is important to recognize that although the spot-Varestraint test is a relatively simple and reproducible test, the direct comparison of quantitative results obtained at different laboratories must be performed with caution due to minor differences in the testing equipment and procedures. In addition, specific alloys actually exhibit a range of cracking susceptibilities due to differences in composition, grain size and heat treatment. Note that the approximate susceptibility of these alloys to liquation cracking increases with their Ti + Nb content.

The weld metal liquation cracking susceptibility of the Alloy 903 was markedly greater than the HAZ liquation cracking of alloys shown in Fig. 13. Unfortunately, Spot-Varestraint data for weld metal liquation cracking in these alloys are not available in the literature. However, this weld metal liquation cracking sensitivity was found to be nearer to HAZ liquation cracking in cast- and heat-treated (1093°C/1999°F, 24 h, WQ) Alloy 718 exhibiting comparable secondary constituent phases and a large grain size (Ref. 12).

[2]*Solution treated at 1065°C (1950°F)/1 h RC + age 718°C (1325°F)/8 h FC to 621°C (1150°F) for 18 h from onset of first age.*

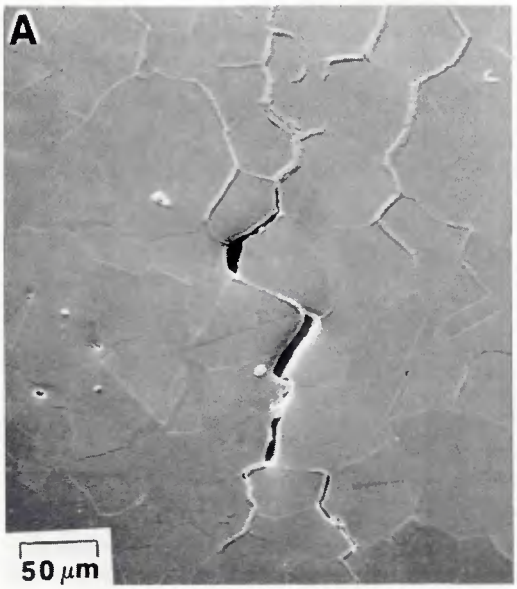

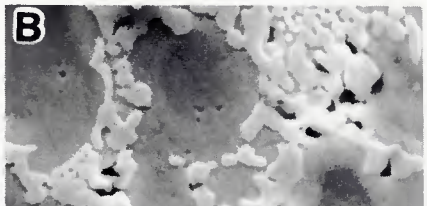

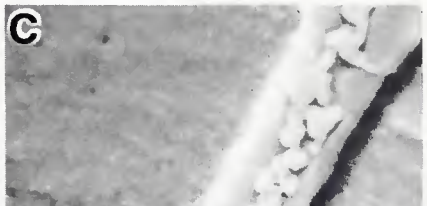

Fig. 9 — SEM micrographs of single-weld Spot-Varestraint specimen tested at 3% augmented strain showing: A — HAZ liquation crack; B — backfilled portion of HAZ liquation crack adjacent fusion line; C — backfilled tip of HAZ liquation crack

Liquation Mechanisms

A prerequisite for HAZ and weld metal liquation cracking is the formation of discrete liquid regions within the solid metal adjacent to the fusion line. If this liquid exhibits a tendency to wet and thereby form a continuous or semi-continuous thin film of liquid along grain boundaries, and if sufficient strains are present in this weld region, then intergranular separation will occur. The origin of such liquation in the weld HAZ is most often attributed to "constitutional liquation" phenomenon, which was originally hypothesized and observed by Savage and co-workers (Refs. 13, 14). This phenomenon involves a eutectic liquation reaction between a secondary constituent phase and the matrix. During the past decade, HAZ liquation in austenitic alloys containing Nb and Ti has been attributed to the constitutional liquation of Nb-rich MC carbides (Refs. 3, 5, 6), Ti-rich MC carbides (Refs. 4, 7), Ti-rich carbonitrides and Laves phase (Refs. 5, 12, 15, 16). Since many alloy microstructures contain more than one secondary constituent phase (*e.g.*, castings and weld metal can contain carbides, carbonitrides and Laves phases), it is important to recognize that constitutional-liquation reactions can involve each of these phases, with liquation initiating at their respective eutectic temperatures. Generally, the phase exhibiting the lowest eutectic reaction temperature dominates the HAZ liquation and contributes greatest to cracking.

In the present study, a constitutional liquation reaction was observed in the HAZ between coarse, Nb-rich carbides and the austenitic matrix. The extent of this reaction ranged from localized interfacial liquation in the far, partially melted region to complete carbide dissolution adjacent to the fusion line. Resolidification of the liquated regions occurred primarily to an austenite/Nb-rich Laves phase eutectic. Such formation of an austenite/Laves phase eutectic concur-

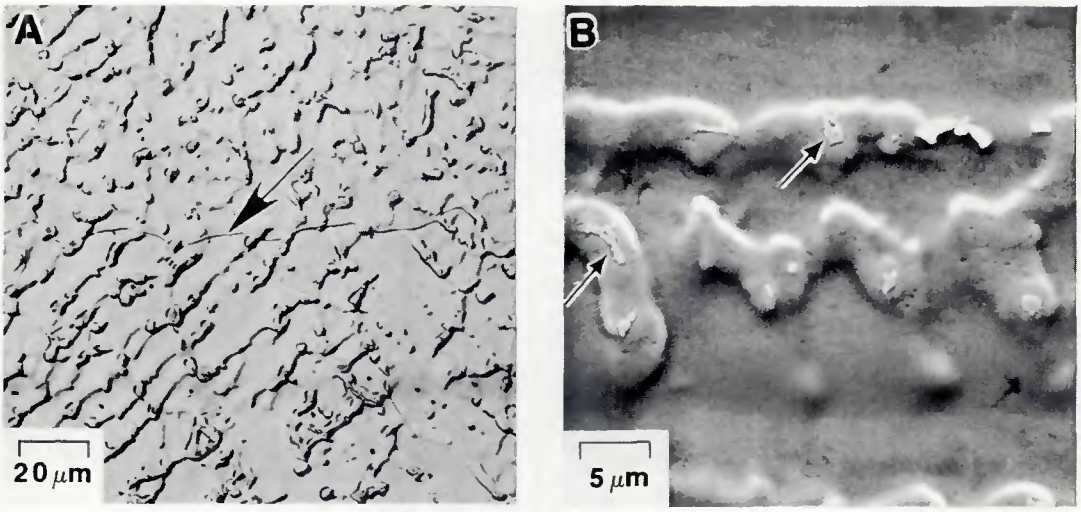

Fig. 10—Micrographs of fusion zone structure in continuous GTA weld. A—Light microscope; B—SEM. Arrow in A indicates austenitic grain boundary. Arrows in B indicate Laves phase

rent with Nb- or Ti-rich carbide constitutional liquation has been reported by Brooks in A-286 (Ref. 4) and Thompson in Alloy 718 (Ref. 6). In Alloy 903, the formation of a Laves/austenite eutectic versus a Nb-rich carbide/austenite eutectic results from the rapid diffusion of carbon away from the liquated region into the surrounding austenitic matrix and the concurrent dilution of the Nb concentration in the liquid via dissolution of the surrounding austenitic matrix. The constitutional liquation of Ti-rich carbonitrides was not visible in the HAZ, which is consistent with the comparably high eutectic reaction temperature of this phase.

Although the liquated carbides were located predominantly intragranularly in the base metal microstructure, austenitic grain growth in the HAZ during the weld thermal cycle promoted impingement of the grain boundaries with the liquated regions. The extent of grain boundary

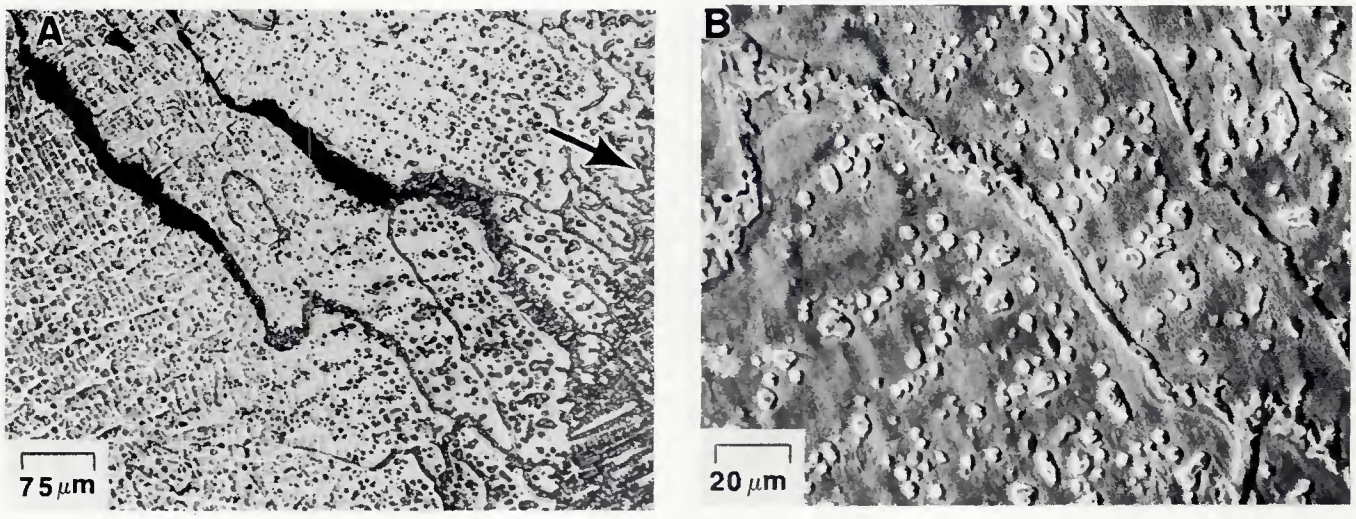

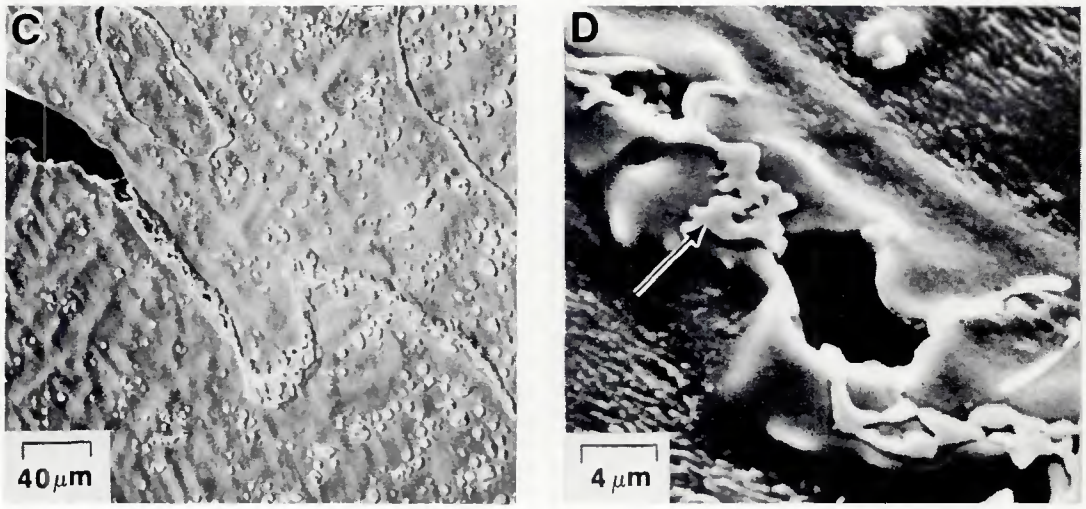

Fig. 11—Light (A) and SEM (B-D) Micrographs of partially-melted region on weld metal side of double-weld spot-Varestraint test specimen tested at 3% augmented strain. A—Light microscope; B to D—SEM. Large arrow in A indicates fusion line. Small arrow in D indicates Laves phase

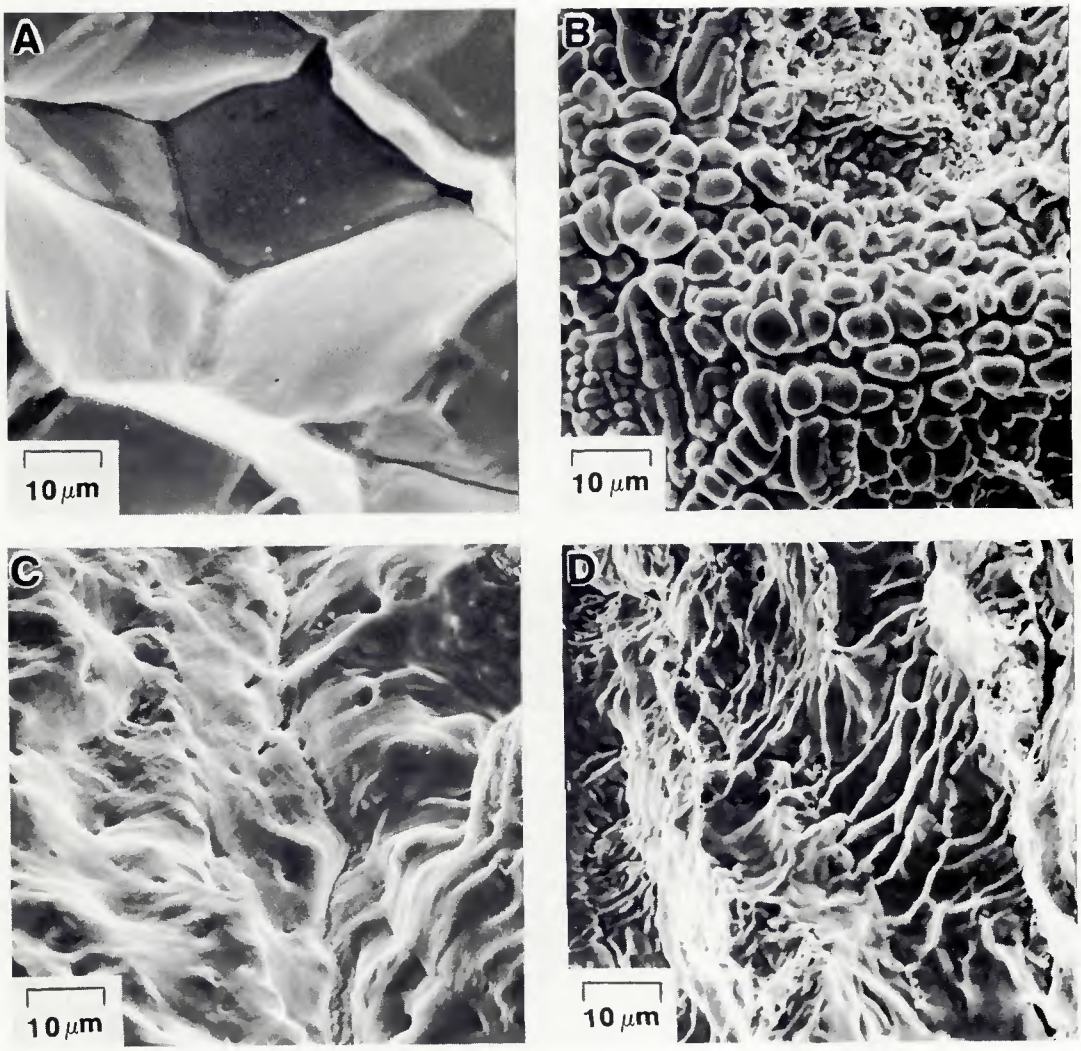

Fig. 12 — SEM fractographs of liquation crack surfaces. A and B — HAZ; C and D — weld metal. Regions in B and D were located adjacent to GTA spot weld fusion line

liquation generally paralleled that of the constitutional liquation reaction, ranging from nearly unresolvable in the far partially melted region near liquation cracks to extensive along grain boundaries adjacent to the fusion line.

The as-welded Alloy 903 microstructure exhibited an austenite/Laves eutectic at solidification substructure (*i.e.*, cellular dendrite) and grain boundaries. In the double-weld Spot-Varestraint specimens, this eutectic liquated along these boundaries, with the degree of both intergranular and intragranular (at substructure boundaries) particularly extensive near the spot weld fusion line. Studies of HAZ liquation cracking in cast Alloy 718 microstructures containing both Nb-rich MC carbides and Laves phase (Ref. 15) have indicated that the Nb-rich Laves phase exhibits a eutectic reaction temperature

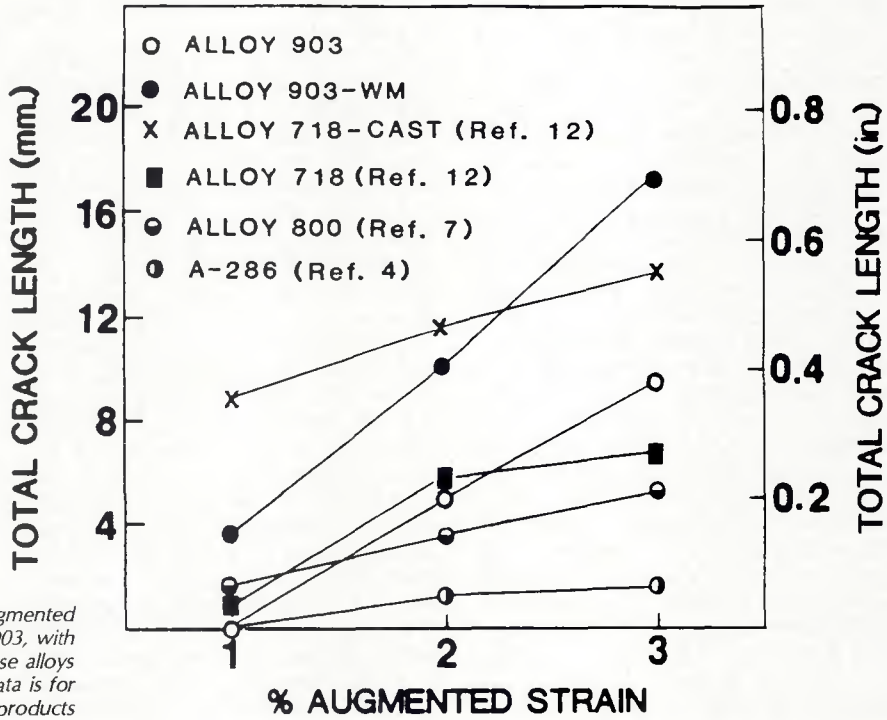

Fig. 13 — Plot comparing TCL to the augmented strain for spot-Varestraint tested Alloy 903, with similar test data for austenitic Fe- and Ni-base alloys containing Cb and/or Ti. Unless noted, data is for base metal liquation cracking in wrought products

appreciably lower than that of the Nb-rich MC carbide. Such a difference was also indicated by hot-ductility testing of cast versus wrought Alloy 718 (Ref. 16), and it was recently confirmed by differential thermal analysis (DTA) studies on wrought Alloy 718 by Cieslak (Ref. 17), who found a Nb-carbide austenite eutectic temperature of 1260°C (2300°F) and a Laves/austenite eutectic temperature of approximately 1200°C (2192°F). Although application of DTA analysis in the present investigation was unable to delineate individual liquation reaction (eutectic) temperatures in Alloy 903, parallels in the microstructure evolution of Alloy 903 and Alloy 718 during welding (despite different matrix chemistries) would suggest a similarly low eutectic temperature for the weld metal Laves phase, relative to the base metal carbides. It is this difference in eutectic temperatures that contributed to the wider region of partial melting observed in the weld metal compared to the base metal HAZ.

Considering the extensive grain boundary liquation observed in the Alloy 903 HAZ and the somewhat limited volume percentage of liquating Nb-rich carbides, it is apparent that additional mechanisms may be operative that enrich HAZ austenitic grain boundaries in Nb.

In addition to constitutional liquation, additional mechanisms have been proposed to explain the origin of HAZ liquation. Recent work by Lippold (Ref. 7) on Incoloy 800 has suggested the possibility of a grain boundary sweeping phenomenon which enriches austenitic grain boundaries in titanium. The origin of this titanium in the matrix is the dissolution of fine Ti-rich MC carbides in the HAZ during the weld thermal cycle. In the present study, fine Nb-rich carbides experienced solid-state dissolution in the HAZ, with their residual Nb-rich diffusion fields rapidly dissipating in the grain-coarsened region. EDS analysis of grain boundaries in the grain-coarsened region, including those adjacent to liquation cracks, however, showed no evidence of Nb-enrichment relative to the matrix. This suggests either an inability of the grain boundaries to accumulate Nb via a sweeping phenomenon, or possibly, the presence of an extremely thin enriched layer undetectable with EDS analysis. Although EDS analysis of fracture surfaces indicated Nb-enrichment, it was not possible to clearly distinguish an as-cracked surface from one in which the original surface had been masked by backfilled liquid. In the case of weld metal liquation cracking, the influence of such a mechanism would appear minimal since the fusion zone solidification boundaries appear to migrate very little from their original position, due to their high inherent stability and to pinning by fine Laves and carbide particles—Fig. 10A.

Liquation Cracking—HAZ versus Weld Metal

In the present investigation, both HAZ and weld metal liquation cracking resulted from an inability of liquated or partially liquated grain boundaries to accommodate stresses produced during Spot-Varestraint testing. Considering the essentially identical base metal and weld metal chemistries, it is apparent that differences in cracking susceptibilities resulted from significant differences in the macro and microstructural characteristics of these two weld regions.

As discussed previously, the lower eutectic reaction temperature of the Laves phase in the weld metal, as compared to the carbide phase in the base metal, promoted a wider region of partial melting. In addition, a greater volume percentage of Laves phase in the weld metal, as opposed to Nb-rich carbides in the HAZ, promoted an increased degree of liquation. These combined effects promoted both a greater total crack length and total number of cracks, particularly at the lower restraint levels. The effect of a wider region of partial melting on cracking was apparent in the significantly greater maximum crack lengths of the weld metal versus the HAZ regions. It is of interest to note that since the austenite/Laves eutectic is ultimately present at grain boundaries in both regions, similar maximum crack lengths might be expected (assuming that maximum crack lengths correlate with the effective solidus). The observed differences in MCL suggest the importance of the quantity and location of the eutectic liquid, and possibly, the grain boundary wetting characteristics, in determining the extent of grain boundary liquation and cracking.

Recent work by Thompson, *et al.* (Ref. 18), has demonstrated the significance of grain size on the liquation cracking sensitivity in wrought Alloy 718. This work was consistent with previous observations of a high-liquation cracking sensitivity in coarse-grained cast Alloy 718 structures (Ref. 12). It is suggested that the significant difference in grain size between the HAZ and weld metal microstructures also contributed to the greater TCL exhibited by the weld metal. It is important to recognize that all of the fusion zone grain boundaries were not cracked, indicating that the TCL had not reached a maximum even at 3% augmented strain.

In addition to austenitic grain size, the tortuosity exhibited by the intergranular liquation crack path may also influence the liquation crack propagation behavior. Such an effect has been suggested by recent work of Brooks, *et al.* (Ref. 19), which demonstrated the importance of crack path tortuosity on the propagation of solidification cracks in austenitic and austenitic/ferritic stainless steels. In the present investigation, the greater MCL and TCL exhibited in the weld metal may in part be attributed to the long, relatively smooth intergranular crack paths. In contrast, the smaller, equiaxed HAZ grain morphology promoted a comparably more irregular crack path.

As discussed previously, the distinction of weld metal liquation cracking is made when it occurs independently of fusion zone solidification cracking. As mentioned earlier, such cracking was observed in Alloy 903 weld cladding (Ref. 9). Based on the present analysis, however, it would be anticipated that Alloy 903 would also be sensitive to weld metal solidification cracking as a result of the formation of the same Laves eutectic film which forms in the HAZ. If such is the case, then the restriction of cracks to the HAZ versus the weld metal is likely a strain-related effect, as opposed to a compositional or microstructural effect.

Conclusions

1) Utilization of a "double-weld" spot-Varestraint test has shown Alloy 903 to be appreciably more susceptible to weld metal cracking rather than HAZ liquation cracking.

2) HAZ liquation involves the constitutional liquation of Nb-rich carbides with the simultaneous formation of a low melting Laves eutectic.

3) Weld metal liquation involves the constitutional liquation of intergranular and interdendritic Laves phase.

4) The greater liquation cracking susceptibility of the weld metal versus the HAZ has been attributed primarily to: 1) a lower eutectic reaction temperature of the weld metal Laves phase relative to the base metal carbides, which promotes a more extensive region of partial melting, 2) a larger austenitic grain size, and 3) a less tortuous liquation crack path.

Acknowledgments

The authors would like to thank Messrs. S. Ernst, I. Varol and P. Wadsworth for their experimental assistance. In addition, appreciation is expressed to Dr. J. C. Lippold of Edison Welding Institute for his comments and review of this manuscript.

References

1. Carpenter, H. W. 1976. Alloy 903 helps space shuttle fly. *Metal Progress* (8):25–29.

2. Smith, D. F., and Clatworthy, E. F. 1981. The development of high strength, low expansive alloys. *Metal Progress* (3):32–35.

3. Duvall, D. S., and Owczarski, W. A. 1967. Further heat-affected zone studies in heat-resistant alloys. *Welding Journal* 46(9): 423-s to 432-s.

4. Brooks, J. A. 1974. Effect of alloy modifications on HAZ cracking of A-286 stainless steel. *Welding Journal* 53(11):517-s to 523-s.

5. Nakao, Y., Oschice, H., Koga, S., Nishihara, H., and Sugitoni, J. 1982. Effect of Nb/C on the sensitivity of liquation cracking in 25Cr-20Ni-1.5Nb Fe base heat resisting alloy. *Journal Japan Welding Society* 51(12):21-27.

6. Thompson, R. G., and Genculu, S., 1983. Microstructural evolution in the HAZ of Inconel 718 and correlation with hot ductility. *Welding Journal* 62(12):337-s to 345-s.

7. Lippold, J. C. 1983. An investigation of heat-affected zone cracking in Alloy 800. *Welding Journal* 62(1):1-s to 11-s.

8. Hemsworth, B., Boniszewski, T., and Eaton, N. F. 1982. Classification and definition of high temperature welding cracks in alloys. *Metal Construction and British Welding Journal* (2):5-16.

9. Betts, R. D. 1975. Incoloy 903 weld overlay study. Internal Report No. MPR75-324, Rockwell International.

10. Lundin, C. 1982. The Varestraint test. Welding Research Council Bulletin No. 280.

11. Pepe, J. J., and Savage, W. F. 1967. Effects of constitutional liquation in 18Ni maraging steel weldments. *Welding Journal* 46(9):411-s to 422-s.

12. Tsay, Y. 1984. An investigation of heat-affected zone cracking in cast Alloy 718. MS Thesis, The Ohio State University, Columbus, Ohio.

13. Dudley, R. H. 1962. Ph.D. Thesis, Rensselaer Polytechnic Institute, Troy, N. Y.

14. Pepe, J. J., and Savage, W. F. 1967. Effects of constitutional liquation in 18Ni maraging steel weldments. *Welding Journal* 46(9): 411-s to 422-s.

15. Baeslack, W. A., III, and Nelson, D. E. 1986. Morphology of weld heat-affected zone liquation in cast alloy 718. *Metallography* 19: 317-379.

16. Nishiyama, V., Vermura, T., Nagai, S., and Morikawa, Y. 1978. *Japan Inst. of Metals* 42:347-356.

17. Cieslak, M. J. 1985. Private communication.

18. Thompson, R. G., Cassimus, J. J., Mayo, D. E., and Dobbs, J. R. 1985. The relationship between grain size and microfissuring in alloy 718. *Welding Journal* 64(4):91-s to 96-s.

19. Brooks, J. A., Thompson, A. W., and Williams, J. C. 1984. A fundamental study of the beneficial effects of delta ferrite in reducing weld cracking. *Welding Journal* 63(3):71-s to 83-s.